Azimuthal Imaginary Poynting Momentum Density

Xiaohao Xu[1,*] and Manuel Nieto-Vesperinas[2]
[1]*Institute of Nanophotonics, Jinan University, Guangzhou 511443, China*
[2]*Instituto de Ciencia de Materiales de Madrid, Consejo Superior de Investigaciones Científicas, Campus de Cantoblanco, Madrid 28049, Spain*

(Received 27 February 2019; published 4 December 2019)

The momentum of light beams can possess azimuthal densities, circulating around the beam axis and inducing intriguing mechanical effects in local light-matter interaction. Belinfante's spin momentum loops in circularly polarized beams, while the canonical momentum spirals in helically phased beams. However, a similar behavior of their imaginary counterpart, the so-called imaginary Poynting momentum (IPM), has not yet emerged. The foremost purpose of the present work is to put forward the discovery of this IPM vortex. We show that a simple superposition of radially and azimuthally polarized beams can form an IPM of completely azimuthal density. Additionally, the azimuthal IPM density can exist with a donut beam-intensity distribution and even with a vanishing azimuthal component of all other momenta. This uncovers the existence of a new mechanical effect which broadens the area of optical micromanipulation by achieving optical rotation of isotropic spheres, in the absence of both spin and orbital angular momenta. Our findings enrich the local dynamic properties of electromagnetic fields, highlighting the rotational action of their IPM, and thus its mechanical effect on microparticles and nanoparticles.

DOI: 10.1103/PhysRevLett.123.233902

The linear momentum carried by a beam of light always aligns along its mean direction of propagation [1]. Nonetheless, local momentum densities can arise in transverse directions and manifest themselves via light-matter interaction [1–6]. When the beam yields azimuthal components to the momentum densities at every azimuthal position, it can set small objects into continuous rotation about its axis via an azimuthal optical force, which offers a distinct degree of freedom to optical micromanipulation [7–15].

Conventionally, the momentum density $\mathbf{P}$ of a monochromatic electromagnetic field is expressed in terms of the time-averaged Poynting vector: $\mathbf{P} = \mathrm{Re}(\mathbf{E}^* \times \mathbf{H})/(2c^2)$ [16]. It can be further decomposed into a canonical or orbital momentum (CM) $\mathbf{P}_O$ derived from phase gradient, and a Belinfante's spin momentum (BSM) $\mathbf{P}_S$ concerning the spin inhomogeneity [14,15,17–21], i.e.,

$$\mathbf{P} = \underbrace{\frac{1}{4\omega n^2}\mathrm{Im}[\varepsilon \mathbf{E}^* \cdot (\nabla)\mathbf{E} + \mu \mathbf{H}^* \cdot (\nabla)\mathbf{H}]}_{\mathbf{P}_O} + \underbrace{\frac{1}{8\omega n^2}\nabla \times \mathrm{Im}(\varepsilon \mathbf{E}^* \times \mathbf{E} + \mu \mathbf{H}^* \times \mathbf{H})}_{\mathbf{P}_S}, \qquad (1)$$

with permittivity ε, permeability μ, and refractive index n of the embedding medium. We know that the azimuthal CM and BSM densities provide the physical origin of the (intrinsic) orbital and spin angular momenta for a paraxial beam, respectively, and hence they can naturally appear in helically phased [1,7–9,22,23] [cf. Fig. 1(a)] and circularly polarized beams [Fig. 1(b)] [13–15,18] carrying their corresponding angular momentum. In this context, it seems that the azimuthal optical force must rely on the CM or the BSM, and, hence, an orbital rotation of objects in the absence of both spin [9] and orbital [13–15] angular momentum is counterintuitive.

However, optical force theory explicitly shows that the imaginary part of the complex Poynting vector $\mathrm{Im}(\mathbf{E}^* \times \mathbf{H})$ is also relevant in the local light-matter momentum exchange [24]. In this regard, the concept of imaginary Poynting momentum (IPM) density, $\mathrm{Im}(\mathbf{\Pi}) = \mathrm{Im}(\mathbf{E}^* \times \mathbf{H})/(2c^2)$, was recently introduced [2–5]. While the quantum-mechanical picture of the IPM has not yet been well established, numerical [2,3] and experimental [4] results have demonstrated that its density $\mathrm{Im}(\mathbf{\Pi})$ is measurable. The IPM density is sensitive to both the intensity inhomogeneity and polarization of the fields

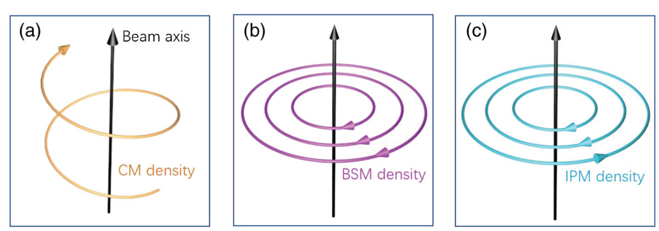

FIG. 1. Illustration for different optical momentum vortices. (a) Canonical momentum in helically phased beams. (b) Belinfante's spin momentum in circularly polarized beams. (c) Imaginary Poynting momentum in cylindrical vector beams.

[2–5,19,25–27]. It can arise in various cases [2–5,25–27] except for plane waves and circularly polarized paraxial beams [19], and its transverse nature is ubiquitous [2–5,19,25,26]. Then an important question is whether $\mathrm{Im}(\mathbf{\Pi})$ can be completely azimuthal, forming a vortex. And if so, whether this vortex can contribute to a spatially global angular momentum of the fields.

In this Letter, we show that the azimuthal IPM density is present in the cylindrical vector beams of donut intensity distribution and spiral polarization. It constitutes a close circulation structure around the beam axis, as illustrated in Fig. 1(c). Depending on the radial position, its direction can be either azimuthal or antiazimuthal, which, as we shall show, makes it to produce a "virtual" angular momentum of nonzero density and vanishing spatially global value. We will evaluate the optical force acting on a probe particle and examine the possibility to realize orbital rotation using this IPM vortex, without the CM and BSM vortices.

The cylindrical vector (CV) beam is created by an in-phase superposition of radially polarized (RP) and azimuthally polarized (AP) beams of special amplitude relation. Analytically, the electric and magnetic fields for AP and RP beams propagating along the z direction in cylindrical coordinates (r, ϕ, z) take the form [cf. Eqs. (2.9)–(2.14) in Ref. [28]]:

$$\mathbf{E}_{\mathrm{AP}} = E_0 U(r,z) e^{ikz} \widehat{\mathbf{e}}_\phi, \qquad \mathbf{H}_{\mathrm{AP}} = -\frac{i}{\mu\omega} \nabla \times \mathbf{E}_{\mathrm{AP}};$$
$$\mathbf{H}_{\mathrm{RP}} = H_0 U(r,z) e^{ikz} \widehat{\mathbf{e}}_\phi, \qquad \mathbf{E}_{\mathrm{RP}} = \frac{i}{\varepsilon\omega} \nabla \times \mathbf{H}_{\mathrm{RP}}; \tag{2}$$

where E_0 and H_0 are amplitude constants, $U(r,z)$ is a paraxial solution to the full wave vector equation, which is ϕ independent. A temporal dependence $\exp(-i\omega t)$ of the fields is considered throughout.

The RP and AP beams have no helical phase structures, nor global spin, because they can be treated as the superposition of two Laguerre-Gaussian beams with equal magnitude, opposite circular polarization, and azimuthal mode index $l = \pm 1$ [29]. We can thus expect that their in-phase superposition will not produce spin and orbital angular momentum [30], and hence no azimuthal BSM nor CM densities. Letting $H_0 = c\varepsilon E_0/n$, the CV beam can be expressed as

$$\begin{aligned} \mathbf{E} &= \mathbf{E}_{\mathrm{AP}} + \mathbf{E}_{\mathrm{RP}} \\ &= \left(E_0 U(\widehat{\mathbf{e}}_r + \widehat{\mathbf{e}}_\phi) + \frac{ic}{n\omega r} E_0 \frac{\partial(rU)}{\partial r} \widehat{\mathbf{e}}_z \right) e^{ikz}, \\ \mathbf{H} &= \mathbf{H}_{\mathrm{AP}} + \mathbf{H}_{\mathrm{RP}} \\ &= \left(\frac{nE_0}{\mu c} U(-\widehat{\mathbf{e}}_r + \widehat{\mathbf{e}}_\phi) - \frac{i}{\mu\omega r} E_0 \frac{\partial(rU)}{\partial r} \widehat{\mathbf{e}}_z \right) e^{ikz}, \end{aligned} \tag{3}$$

which constitutes a decomposition of the fields into longitudinal and transversal components (see, e.g., [31] on the relevance of such kind of decomposition of the wave fields). To derive (3), we have ignored $\partial U/\partial z$ compared with kU, which is a correct assumption for a paraxial beam whose transverse profile changes slowly with position z along the propagation direction [23,31].

Using (3), the complex Poynting momentum density [3] for the CV beam is readily obtained in terms of its longitudinal and transversal components:

$$\begin{aligned} \Pi &= \frac{1}{2c^2} (\mathbf{E}^* \times \mathbf{H}) \\ &= \frac{E_0^2}{\mu\omega c^2} \mathrm{Im}\left(U^* \frac{\partial U}{\partial r} \right) \widehat{\mathbf{e}}_r \\ &\quad - \frac{iE_0^2}{2\mu\omega r c^2} \left(2|U|^2 + r \frac{\partial |U|^2}{\partial r} \right) \widehat{\mathbf{e}}_\phi + \frac{n}{\mu c^3} E_0^2 |U|^2 \widehat{\mathbf{e}}_z. \end{aligned} \tag{4}$$

Then the time-averaged momentum density can be expressed as [2,3,16]:

$$\mathbf{P} = \mathrm{Re}(\mathbf{\Pi}) = \frac{E_0^2}{\mu\omega c^2} \mathrm{Im}\left(U^* \frac{\partial U}{\partial r} \right) \widehat{\mathbf{e}}_r + \frac{n}{\mu c^3} E_0^2 |U|^2 \widehat{\mathbf{e}}_z. \tag{5}$$

The radial component is small, and it vanishes at the beam waist plane where U is real valued [28]. Additionally, the paraxial spin-orbital decomposition [31,32] yields $\mathbf{P}_O = \mathbf{P}$ and $\mathbf{P}_S = 0$.

In this Letter, we will focus on the IPM density:

$$\mathrm{Im}(\mathbf{\Pi}) = -\frac{E_0^2}{2\mu\omega c^2 r} \left(2|U|^2 + r \frac{\partial |U|^2}{\partial r} \right) \widehat{\mathbf{e}}_\phi, \tag{6}$$

which in contrast with its real part Eq. (5), has no longitudinal component, possessing an azimuthal one only. This special directionality is accompanied by a vanishing divergence $\nabla \cdot \mathrm{Im}(\Pi) = 0$. In this connection, one should note that the IPM is not divergenceless in most cases [2–5,19,25–27]. On multiplying $\mathrm{Im}(\mathbf{\Pi})$ by a radius vector $\mathbf{r}$ from the axis, we arrive at a pseudovector with a dimension of angular momentum density

$$\mathbf{R} = \mathbf{r} \times \mathrm{Im}(\mathbf{\Pi}) = -\frac{E_0^2}{2\mu\omega c^2} \left(2|U|^2 + r \frac{\partial |U|^2}{\partial r} \right) \widehat{\mathbf{e}}_z. \tag{7}$$

We coin $\mathbf{R}$ as the density of a reactive angular momentum (RAM), which is the imaginary counterpart of the time-averaged angular momentum density [23]:

$$\mathbf{M} = \mathbf{r} \times \mathbf{P} = -\frac{nr}{\mu c^3} E_0^2 |U|^2 \widehat{\mathbf{e}}_\phi. \tag{8}$$

The mechanical effects of the IPM density, like that of the BSM density [2,3], cannot be felt by purely electric, or purely magnetic, dipolar particles [33]. However, it acts on magnetodielectric particles, namely those supporting both electric and magnetic moments induced by the electric and magnetic vectors of the illuminating wave [2–6,24]. For simplicity, we shall focus on its role in the generic dipolar interaction of light with an isotropic particle, which can be found in the magnetoelectric interference force [24]

$$\mathbf{F} = \frac{8\pi c \mu_r^2 k^4}{3n}[\mathrm{Im}(\alpha_e \alpha_m^*)\mathrm{Im}(\mathbf{\Pi}) - \mathrm{Re}(\alpha_e \alpha_m^*)\mathbf{P}], \quad (9)$$

with $\mu_r = \mu/\mu_0$ being the relative permeability of the medium, while α_e and α_m are the electric and magnetic polarizabilities of the dipoles induced in the particle. It follows that there is an azimuthal force acting on the particle for the vector beam, i.e.,

$$\begin{aligned}\mathbf{F}_\phi &= \frac{8\pi c \mu_r^2 k^4}{3n}[\mathrm{Im}(\alpha_e \alpha_m^*)\mathrm{Im}(\mathbf{\Pi}_\phi)] \\ &= -\frac{4\pi \mu_r^2 k^3 E_0^2}{3\mu c^2 r}\mathrm{Im}(\alpha_e \alpha_m^*)\left(2|U|^2 + r\frac{\partial |U|^2}{\partial r}\right)\hat{\mathbf{e}}_\phi, \quad (10)\end{aligned}$$

which is provided solely by the IPM, and constitutes a force moment continuously rotating the particle.

To show the IPM vortex and its rotational mechanical effects, simulations are performed by using the finite-difference time-domain method. A common expression is used for describing the beam profile [28,34]: $U(r,z) = [r/(w\xi^2)]\exp[-r^2/(w^2\xi)]$, where the complex parameter ξ is $\xi = 1 + iz\lambda/(2\pi w^2)$. The waist size w and wavelength λ are set to be $w = 1\ \mu$m and $\lambda = 600$ nm, for which the paraxial theory is valid at $r \le 2\ \mu$m as $|\partial U/\partial z|/|kU| \le 0.018 \ll 1$ [35]. Figure 2 shows the field distribution at the waist plane ($z = 0$) of the CV beam propagating in water. The field is axially symmetric, with a ringlike intensity pattern and spiral polarization [cf. Fig. 2(a)]. The axial CM density [cf. Fig. 2(b)] and negligible BSM density (not shown), suggest that the field carries no spin nor orbital angular momentum. Remarkably, the IPM density completely aligns in the azimuthal direction [Figs. 2(c) and 2(d)]. The azimuthal component preserves constant signs at $r < 1\ \mu$m, but changes at $r > 1\ \mu$m. This should be caused by its intensity inhomogeneity-related term [cf. Eq. (6)].

To observe the azimuthal force, high-index dielectric (e.g., Si and GaAs) nanoparticles can be used, as they have both dipolar electric and magnetic responses to the incident electromagnetic wave [36–40]. As an example, Fig. 3 shows the time-averaged optical forces acting on a Si sphere of radius: 70 nm as its radial position varies at the waist plane of the CV beam, which are calculated through the Maxwell stress tensor [16]. The refractive index of Si is adopted from the experimental data of Ref. [41].

Thanks to the annular intensity profile, the particle experiences a radial restoring force F_r, which results from the intensity gradient [33,42] [see also Eqs. (42) and (43) in Ref. [24]], and tends to confine the sphere at $r = 0.7\ \mu$m. As expected from our previous analysis, the azimuthal force F_ϕ arises, and its magnitude is remarkable comparing it with the radial force. It exhibits a trend similar to that of $\mathrm{Im}(\prod_\phi)$ [cf. Fig. 2(c)] as the radial position of the particle varies in the beam waist. On the other hand, F_ϕ is nonzero at $r = 0.7\ \mu$m (i.e., at the radial equilibrium position), which ensures rotation of the sphere when radial trapping occurs.

The fact that Si (and other high-index magnetoelectric) spheres can be rotated in water is important for experiments, as this offers us a procedure to accurately measure the local IPM by directly observing the periodic motion (or rotation) velocity of such an isotropic spherical probe.

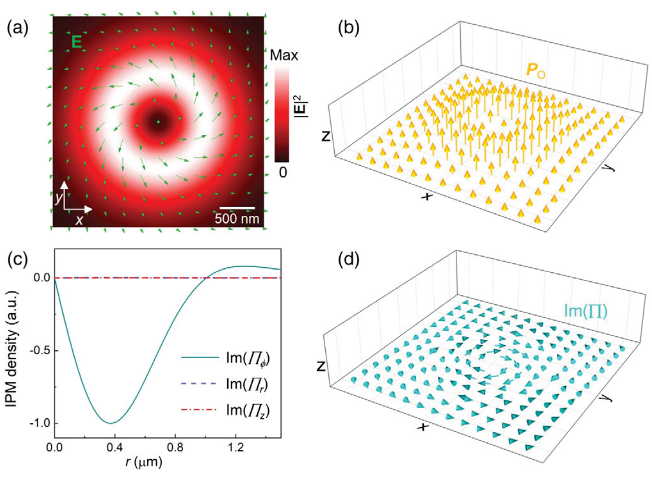

FIG. 2. Simulated field transversal spatial distribution at the waist plane of a cylindrical vector beam. (a) Intensity distribution with arrows indicating the polarization direction. (b) CM density. (c) Radial, azimuthal, and axial components of the IPM density versus the radial position. (d) IPM vortex.

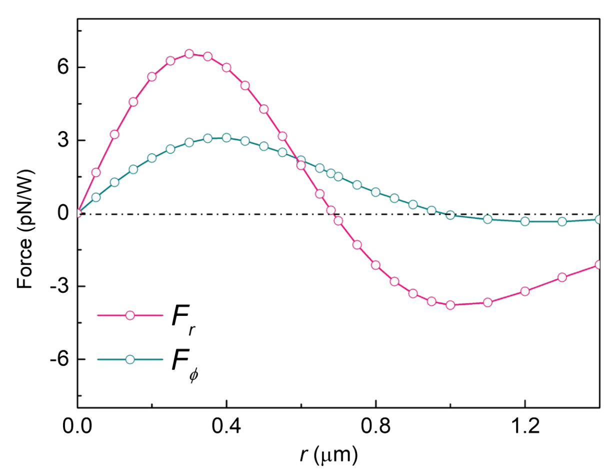

FIG. 3. Radial variation of the optical forces on a silicon sphere (diameter: 140 nm), located at the waist plane of the cylindrical vector beam shown in Fig. 2. The illumination wavelength is $\lambda = 600$ nm.

Finally, we must point out that, despite the local RAM originating from the azimuthal IPM density, it does not lead to a global angular momentum. In fact, it is easy to verify that the integral of the RAM density over the whole beam cross section yields a zero value,

$$\int_0^{2\pi}\int_0^{\infty} r\mathbf{R}\, dr\, d\phi \sim \int_0^{2\pi}\int_0^{\infty}\left(2r|U|^2 + r^2\frac{\partial |U|^2}{\partial r}\right) dr\, d\phi = 0, \tag{11}$$

as $r^2|U|^2 = 0$ for $r \to \infty$. Obviously, the positive azimuthal IPM densities at $r > 1\ \mu$m compensate the RAM accumulated by the negative azimuthal IPM densities at $r < 1\ \mu$m [cf. Fig. 2(c)]. Therefore, it can be seen that the RAM is a virtual quantity for the vector beam.

In summary, we have analyzed the vector field created with the in-phase superposition of radially and azimuthally polarized beams of equal magnitude, and found that such a field reveals a nontrivial vortex structure, namely the azimuthal IPM density. Thus, the azimuthal IPM density, along with the azimuthal CM [1,7–9,22,23] and BSM [13–15,18] densities, completes the set of all possible momentum vortices in electromagnetic fields. Its unique direction indicates that the mechanical effect of this momentum can be exploited to continuously rotate objects. This constitutes a new mechanism for light-driven rotation of objects, since such rotation does not rely on the optical spin nor orbital angular momenta, neither the use of inhomogeneous nor anisotropic objects.

This work was supported by the National Natural Science Foundation of China (No. 11804119) and the Ph.D. Start-up Fund of Natural Science Foundation of Guangdong Province (No. 2018A030310502). M. N.-V. acknowledges Spanish Ministerio de Ciencia, Innovación y Universidades, Grants No. FIS2014-55563-REDC, No. FIS2015-69295-C3-1-P, and No. PGC2018-095777-B-C21.

*Corresponding author.
xuxhao@jnu.edu.cn

[1] F. C. Speirits and S. M. Barnett. Do Waves Carrying Orbital Angular Momentum Possess Azimuthal Linear Momentum?, Phys. Rev. Lett. **111**, 103602 (2013).

[2] K. Y. Bliokh, A. Y. Bekshaev, and F. Nori, Extraordinary momentum and spin in evanescent waves, Nat. Commun. **5**, 3300 (2014).

[3] A. Y. Bekshaev, K. Y. Bliokh, and F. Nori, Transverse Spin and Momentum in Two-Wave Interference, Phys. Rev. X **5**, 011039 (2015).

[4] M. Antognozzi *et al.*, Direct measurements of the extraordinary optical momentum and transverse spin-dependent force using a nano-cantilever, Nat. Phys. **12**, 731 (2016).

[5] A. Y. Bekshaev, Dynamical characteristics of an electromagnetic field under conditions of total reflection, J. Opt. **20**, 045604 (2018).

[6] K. Y. Bliokh, Y. S. Kivshar, and F. Nori, Magnetoelectric Effects in Local Light-Matter Interactions, Phys. Rev. Lett. **113**, 033601 (2014).

[7] M. Padgett and R. Bowman, Tweezers with a twist, Nat. Photonics **5**, 343 (2011).

[8] M. J. Padgett, Orbital angular momentum 25 years on, Opt. Express **25**, 11265 (2017).

[9] V. Garcés-Chávez, D. McGloin, M. J. Padgett, W. Dultz, H. Schmitzer, and K. Dholakia, Observation of the Transfer of the Local Angular Momentum Density of a Multiringed Light Beam to an Optically Trapped Particle, Phys. Rev. Lett. **91**, 093602 (2003).

[10] K. Ladavac and D. G. Grier, Microoptomechanical pumps assembled and driven by holographic optical vortex arrays, Opt. Express **12**, 1144 (2004).

[11] J. Leach, H. Mushfique, R. di Leonardo, M. Padgett, and J. Cooper, An optically driven pump for microfluidics, Lab Chip **6**, 735 (2006).

[12] F. Han, J. A. Parker, Y. Yifat, C. Peterson, S. K. Gray, N. F. Scherer, and Z. Yan, Crossover from positive to negative optical torque in mesoscale optical matter, Nat. Commun. **9**, 4897 (2018).

[13] D. B. Ruffner and D. G. Grier, Optical Forces and Torques in Nonuniform Beams of Light, Phys. Rev. Lett. **108**, 173602 (2012).

[14] O. V. Angelsky, A. Ya. Bekshaev, P. P. Maksimyak, A. P. Maksimyak, S. G. Hanson, and C. Yu. Zenkova, Orbital rotation without orbital angular momentum: Mechanical action of the spin part of the internal energy flow in light beams, Opt. Express **20**, 3563 (2012).

[15] V. Svak, O. Brzobohatý, M. Šiler, P. Jákl, J. Kaňka, P. Zemánek, and S. H. Simpson, Transverse spin forces and nonequilibrium particle dynamics in a circularly polarized vacuum optical trap, Nat. Commun. **9**, 5453 (2018).

[16] J. D. Jackson, *Classical Electrodynamics* (Wiley, New York, 1962).

[17] F. J. Belinfante, On the current and the density of the electric charge, the energy, the linear momentum and the angular momentum of arbitrary fields, Physica (Utrecht) **7**, 449 (1940).

[18] A. Bekshaev, K. Y. Bliokh, and M. Soskin, Internal flows and energy circulation in light beams, J. Opt. **13**, 053001 (2011).

[19] A. Bekshaev, Subwavelength particles in an inhomogeneous light field: Optical forces associated with the spin and orbital energy flows, J. Opt. **15**, 044004 (2013).

[20] M. Nieto-Vesperinas, Optical torque: Electromagnetic spin and orbital-angular momentum conservation laws and their significance, Phys. Rev. A **92**, 043843 (2015).

[21] D. Gao, W. Ding, M. Nieto-Vesperinas, X. Ding, M. Rahman, T. Zhang, C. Lim, and C.-W. Qiu, Optical manipulation from the microscale to the nanoscale: Fundamentals, advances and prospects, Light Sci. Appl. **6**, e17039 (2017).

[22] M. D. Williams, M. M. Coles, D. S. Bradshaw, and D. L. Andrews, Direct generation of optical vortices, Phys. Rev. A **89**, 033837 (2014).

[23] L. Allen, M. W. Beijersbergen, R. J. C. Spreeuw, and J. P. Woerdman, Orbital angular momentum of light and the transformation of Laguerre-Gaussian laser modes, Phys. Rev. A **45**, 8185 (1992).

[24] M. Nieto-Vesperinas, J. J. Sáenz, R. Gómez-Medina, and L. Chantada, Optical forces on small magnetodielectric particles, Opt. Express **18**, 11428 (2010).

[25] L. Wei, M. F. Picardi, J. J. Kingsley-Smith, A. V. Zayats, and F. J. Rodríguez-Fortuño, Directional scattering from particles under evanescent wave illumination: The role of reactive power, Opt. Lett. **43**, 3393 (2018).

[26] L. Wei, A. V. Zayats, and F. J. Rodríguez-Fortuño, Interferometric Evanescent Wave Excitation of a Nanoantenna for Ultrasensitive Displacement and Phase Metrology, Phys. Rev. Lett. **121**, 193901 (2018).

[27] R. Gómez-Medina, M. Nieto-Vesperinas, and J. J. Sáenz, Nonconservative electric and magnetic optical forces on submicron dielectric particles, Phys. Rev. A **83**, 033825 (2011).

[28] Q. Zhan, Cylindrical vector beams: From mathematical concepts to applications, Adv. Opt. Photonics **1**, 1 (2009).

[29] The RP and AP beams can be expressed in terms of the LG_{01} modes, for $\hat{\mathbf{e}}_r \sim (\hat{\mathbf{e}}_+ e^{-i\phi} + \hat{\mathbf{e}}_- e^{i\phi})$ and $\hat{\mathbf{e}}_\phi \sim (\hat{\mathbf{e}}_+ e^{-i\phi} - \hat{\mathbf{e}}_- e^{i\phi})$, where $\hat{\mathbf{e}}_+$ and $\hat{\mathbf{e}}_-$ are unit vectors representing opposite circular polarizations. The two formulas provide a physical insight in why the RP and AP beams do not possess angular momentum: both are the simple superposition of two LG_{01} beams whose spins or transverse phase gradients can offset each other.

[30] J. S. Eismann, M. Neugebauer, and P. Banzer, Exciting a chiral dipole moment in an achiral nanostructure, Optica **5**, 954 (2018).

[31] M. V. Berry, Optical currents, J. Opt. **11**, 094001 (2009).

[32] A. Y. Bekshaev and M. S. Soskin, Transverse energy flows in vectorial fields of paraxial beams with singularities, Opt. Commun. **271**, 332 (2007).

[33] P. C. Chaumet and M. Nieto-Vesperinas, Time-averaged total force on a dipolar sphere in an electromagnetic field, Opt. Lett. **25**, 1065 (2000).

[34] V. Shvedov, A. R. Davoyan, C. Hnatovsky, N. Engheta, and W. Krolikowski, A long-range polarization-controlled optical tractor beam, Nat. Photonics **8**, 846 (2014).

[35] It is easy to evaluate the ratio: $\sigma = |\partial U/\partial z|/|kU| = \lambda^2|r^2 - 2\xi w^2|/(4\pi^2\xi^2 w^4)$, which, at the waist plane ($z = 0$, $\xi = 1$), takes the form $\sigma = \lambda^2|r^2 - 2w^2|/(4\pi^2 w^4)$. In our case ($\lambda = 0.6\ \mu$m, $w = 1\ \mu$m), it can be verified that $\sigma \leq 0.018 \ll 1$ (and therefore $|(\partial U/\partial z| \ll |kU|)$ is valid for $r \leq 2\ \mu$m (we are not interested in the case of $r > 2\ \mu$m, where the field almost vanishes). Therefore, the U function employed in our numerical calculation does not violate the paraxial approximation, and thus the numerical results can be used to support the analytical results.

[36] A. B. Evlyukhin, C. Reinhardt, and B. N. Chichkov, Multipole light scattering by nonspherical nanoparticles in the discrete dipole approximation, Phys. Rev. B **84**, 235429 (2011).

[37] A. García-Etxarri, R. Gómez-Medina, L. S. Froufe-Pérez, C. López, L. Chantada, F. Scheffold, J. Aizpurua, M. Nieto-Vesperinas, and J. J. Sáenz, Strong magnetic response of submicron silicon particles in the infrared, Opt. Express **19**, 4815 (2011).

[38] M. Nieto-Vesperinas, R. Gomez-Medina, and J. J. Saenz, Angle-suppressed scattering and optical forces on submicrometer dielectric particles, J. Opt. Soc. Am. A **28**, 54 (2011).

[39] A. I. Kuznetsov, A. E. Miroshnichenko, Y. H. Fu, J. Zhang, and B. Lukyanchuk, Magnetic light, Sci. Rep. **2**, 492 (2012).

[40] A. I. Kuznetsov, A. E. Miroshnichenko, M. L. Brongersma, Y. S. Kivshar, and B. Lukyanchuk, Optically resonant dielectric nanostructures, Science **354**, aag2472 (2016).

[41] M. A. Green and M. J. Keevers, Optical properties of intrinsic silicon at 300 K, Prog. Photovoltaics **3**, 189 (1995).

[42] A. Ashkin, J. M. Dziedzic, J. E. Bjorkholm, and S. Chu, Observation of a single-beam gradient force optical trap for dielectric particles, Opt. Lett. **11**, 288 (1986).